Simulation of surface defects

1994 J. Phys.: Condens. Matter 6 9495

(http://iopscience.iop.org/0953-8984/6/45/004)

J. Phys.: Condens. Matter 6 (1994) 9495–9517. Printed in the UK

REVIEW ARTICLE

Simulation of surface defects

Per Stoltze

Centre for Atomic-Scale Materials Physics and Physics Department, Building 307, Technical University of Denmark, DK-2800 Lyngby, Denmark

Received 8 July 1994, in final form 19 August 1994

Abstract. The energetics of some surface defects for the (100), (110), and (111) surfaces of Cu, Ag, Au, Ni, Pd, and Pt are studied using effective medium theory. Among the calculated data are the surface energy, the energetics of some reconstructions, the formation energy for steps and islands, and the activation energy for diffusion of adatoms.

1. Introduction

In recent years, simulations have become a supplement to theoretical and experimental approaches in solid state and materials physics. In principle, simulations consist of a numerical solution of an equation of motion followed by determination of structural, thermodynamic, and kinetic data through statistical treatment of the results.

For realistic simulations we need a prescription for the calculation of interactions between atoms. The size and complexity of the systems we can treat in a simulation is determined by the available computational power and simulations of physical systems from first principles are only possible using present computer technology for relatively small systems. Approximations are usually required to reduce the computational effort and the introduction of approximations makes experimental input a necessity to validate the approximations through reproduction of suitable, unambiguous experimental results.

The results of simulations may contribute to theory by mapping out the macroscopic effects of changes in the interactions between atoms, or by mapping out the relative importance of different mechanisms. Detailed simulations using approximate methods may also help in the analysis and interpretation of *ab initio* calculations. Simulations may contribute to experimental studies by detailed analysis of the output from simulations of complicated or controversial experiments. Although simulations may contribute to both theory and experiments, the most important result of simulations is undoubtedly the development of intuition and ideas through interactive simulations of a phenomenon under study.

If simulations are to become a tool available not just to experts, the development of interactive and effective simulation programs is necessary. Further the development of accurate, but computationally effective, interaction potentials is required. The overall goal is to develop potentials that retain the essential physics while the computational effort is reduced to a level where interactive simulations of large, disordered systems become feasible.

In the following we will illustrate the application of interactive simulations through computation of the stability of surface defects and the activation energy for diffusion on the

0953-8984/94/459495+23$19.50

(100), (110), and (111) faces of Cu, Ag, Au, Ni, Pd, and Pt based on the *effective medium theory* (EMT).

After a very brief outline of effective medium theory in section 2, we calculate the thermal expansion coefficient for the bulk metals and the surface energy and the surface relaxation for the 18 surfaces and use the comparison with experiment (for the bulk) and with first principle calculations (for the surfaces) to estimate the quality of the results obtained from the simulations. We then proceed to extensive calculations of the energetics of surface defects and of the activation energy for diffusion of adatoms. Many of the latter results would be very difficult to obtain through first principle calculations.

2. Effective medium theory

Effective medium theory [1, 2] (EMT) is an attempt to retain the essential physics for interaction between atoms in metallic systems, while the computational effort is reduced enormously.

EMT is a hierarchy of approximations [1, 3, 4] rather than a single prescription for the calculation of interactions between atoms. In the following we will consider one-component metallic systems and the lowest, most approximate, level of EMT is applicable in this situation. In their form appropriate for the treatment of one-component metallic systems, *effective medium theory* [1, 2], *corrected effective medium theory* [5], the *embedded atom method* (EAM) [6], the *glue model* [7], and other approximate, many-body potentials [8, 9] are equivalent, although the actual implementation may differ substantially.

In this section we will try to give an exposition of how EMT is applied in simulations. [1, 2, 3, 4] contain the derivation and analysis of EMT.

For simple metals the potential energy of the system is

$$E = \sum_i E_c(i) + \Delta E_{AS}(i) \tag{1}$$

where $E_c(i)$ is the embedding energy of atom i in a homogeneous electron gas, $\Delta E_{AS}(i)$ is the atomic sphere correction term, and the summation runs over all atoms in the ensemble.

For each atom

$$E_c(s) = E_0(1 + \lambda(s - s_0))\exp(-\lambda(s - s_0)) \tag{2}$$

and

$$E_{AS} = 6V_0 \exp(\kappa s_0)\left(\left(\frac{\sigma_1}{12\gamma_1}\right)^{\kappa/\beta\eta_2} - \frac{\sigma_2}{12\gamma_2}\right) \tag{3}$$

The Wigner–Seitz radius, s, is

$$s = -\frac{1}{\beta\eta_2}\log\left(\frac{\sigma_1}{12\gamma_1}\right) \tag{4}$$

and σ_1 and σ_2 are calculated by summation over the neighbours of the atom

$$\sigma_1 = \sum_{j\neq i} \theta(r_{ij})\exp(-\eta_2 r_{ij}) \tag{5}$$

$$\sigma_2 = \sum_{j\neq i} \theta(r_{ij})\exp\left(-\frac{\kappa}{\beta} r_{ij}\right). \tag{6}$$

The cut-off function $\theta(r)$ is given by

$$\theta(r) = (1 + \exp(a(r - r_c)))^{-1} \tag{7}$$

where r_c is the cut-off radius and a determines the steepness of the cut-off.

In these equations, η_2 and κ are inverse screening lengths. β is a constant of geometric origin,

$$\beta = \left(\frac{16\pi}{3}\right)^{1/3}\left(\frac{1}{2}\right)^{1/2}. \tag{8}$$

γ_1 and γ_2 are normalization factors allowing for the extension of the summation in equations (5) and (6) to include remote-neighbour pairs. Throughout this study we will assume that γ_1 and γ_2 are functions of the cut-off only. In a perfect FCC structure at optimum lattice constant, $E_c = E_0$ and $E_{AS} = 0$. This defines γ_1 and γ_2 in terms of the cut-off [1].

The average electron density, $\bar{n}$, is related to the Wigner–Seitz radius by

$$\bar{n}(s) = n_0 \exp(-\eta(s - s_0)). \tag{9}$$

n_0 is determined from self-consistent calculations of the atom in a homogeneous electron gas.

The other parameters may be determined from self-consistent calculations or from experimental data using the following equations. The equilibrium, zero-temperature lattice constant for FCC metals is

$$a = \beta s_0 \sqrt{2}. \tag{10}$$

The cohesive energy is

$$E_c = -E_0 \tag{11}$$

the bulk modulus is

$$B = \frac{-E_0 \lambda^2}{12\pi s_0} \tag{12}$$

and the shear modulus is

$$C_{44} = \frac{3V_0\kappa(\beta\eta_2 - \eta)}{8\pi s_0} \tag{13}$$

The parameters used in the following are listed in table 1. The parameters calculated from experimental structural and elastic data give somewhat different simulation results than do the parameters determined from first-principles calculations [10]. One cannot say that one or the other set of parameters is best; they represent different approaches to the determination of the parameters and the differences in the results obtained from the parameters is a reflection of the approximate nature of the EMT potential.

Table 1. EMT parameters.

	E_0 (eV)	s_0 (Bohr)	V_0 (eV)	η_2 (Bohr^{-1})	κ (Bohr^{-1})	λ (Bohr^{-1})	n_0
Cu	−3.51	2.67	2.476	1.652	2.740	1.906	0.00910
Ag	−2.96	3.01	2.132	1.652	2.790	1.892	0.00547
Au	−3.80	3.00	2.321	1.674	2.873	2.182	0.00703
Ni	−4.44	2.60	3.673	1.669	2.757	1.948	0.01030
Pd	−3.90	2.87	2.773	1.818	3.107	2.155	0.00688
Pt	−5.85	2.90	4.067	1.812	3.145	2.192	0.00802

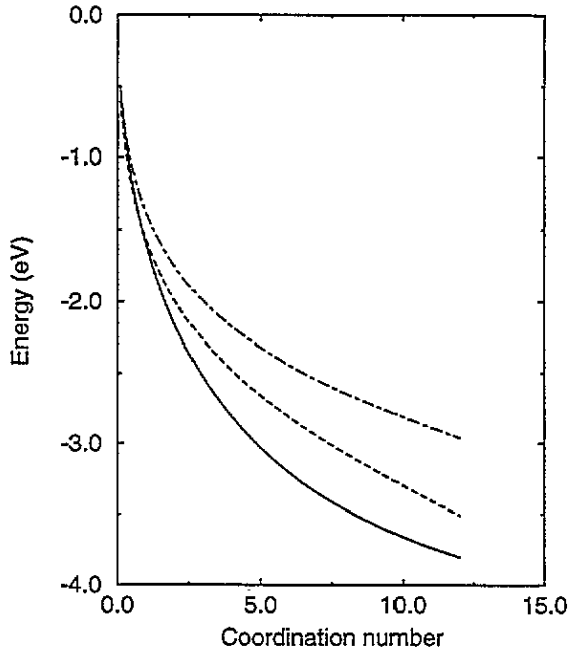

Figure 1. Total energy for atoms as a function of coordination number for Cu (dashed), Ag (dot–dashed), and Au (solid line).

EMT has been applied to the calculation of surface energies [11], surface relaxation [12, 13, 14, 15], stability of surface defects [16, 17], stability of islands [18, 19], and surface phonon spectra [14].

EMT has also been used in studies of surface reconstruction [12, 13, 15], anharmonic effects [14, 20, 21], surface diffusion mechanisms [10, 22, 19], and homoepitaxy [19].

Finally, EMT has been used in simulations of small clusters [21, 23], absorption of H in Pd [24, 25], alloy phase diagrams [26], premelting of flat surfaces [27, 28, 29, 30] and of clusters [31], and in simulations of diffusion on premelted surfaces [32].

3. Bulk properties

For some property $A(\boldsymbol{r}, \boldsymbol{p})$ the canonical average $\langle A \rangle$ is given by

$$\langle A \rangle = Z^{-1} \int A(\boldsymbol{r}, \boldsymbol{p}) \exp\left(-\frac{\epsilon(\boldsymbol{r}, \boldsymbol{p})}{k_B T}\right) \mathrm{d}\boldsymbol{r}\, \mathrm{d}\boldsymbol{p} \tag{14}$$

$$Z = \int \exp\left(-\frac{\epsilon(\boldsymbol{r}, \boldsymbol{p})}{k_B T}\right) \mathrm{d}\boldsymbol{r}\, \mathrm{d}\boldsymbol{p}. \tag{15}$$

If ϵ contains both kinetic and potential energy

$$\epsilon = u(\boldsymbol{r}) + \sum \frac{p^2}{2m} \tag{16}$$

Z will factorize

$$Z = (2\pi m k_B T)^{3N/2} \int \exp\left(-\frac{u(\boldsymbol{r})}{k_B T}\right) \mathrm{d}\boldsymbol{r} \tag{17}$$

where the configuration integral

$$Q(r) = \int \exp\left(-\frac{u(r)}{k_B T}\right) dr \tag{18}$$

is the difficult part. From equation (17) we find that the heat capacity, C_v, contains a contribution, C_v', from the potential energy and a contribution $\frac{3}{2}k_B$ from the kinetic energy

$$C_v = C_v' + \tfrac{3}{2}k_B. \tag{19}$$

The kinetic energy will contribute $\frac{3}{2}k_B$ to the heat capacity. As the kinetic energy is not included in the Monte Carlo simulation, this contribution must be added to the heat capacity determined directly from the Monte Carlo simulation. For a harmonic lattice we expect $C_v = 3k_B$. If anharmonicity is present, C_v will be larger. In the present simulations we expect that the anharmonicity is moderate and C_v is then independent of temperature.

The thermal expansion and the heat capacity were determined from Monte Carlo simulations using 216 atoms in a dynamic box at zero external pressure. For each metal, five simulations were made at temperatures from 8 to 96 meV. In each simulation 101 configurations were generated at each of the temperatures, consecutive configurations were separated by two attempted random displacements per atom, and the amplitudes of the displacements were adjusted to approximately 50% acceptance.

Table 2. Cohesive energy, E_c, heat capacity, C_p, lattice constant, a, thermal expansion coefficient, α_s, and the ratio between the thermal expansion coefficient from simulation, α_s, and experiment, α_e.

	E_c (eV)	C_p (k_B)	a (Bohr)	α_s (ppm K^{-1})	α_s/α_e
Cu	-3.514 ± 0.002	3.173 ± 0.038	6.771 ± 0.014	22.1 ± 0.8	1.3
Ag	-2.964 ± 0.004	3.324 ± 0.068	7.654 ± 0.039	31.8 ± 2.0	1.7
Au	-3.793 ± 0.007	2.722 ± 0.124	7.657 ± 0.032	18.2 ± 1.6	1.3
Ni	-4.445 ± 0.002	3.099 ± 0.040	6.579 ± 0.008	14.9 ± 0.5	1.1
Pd	-3.904 ± 0.004	3.293 ± 0.078	7.310 ± 0.035	24.1 ± 1.9	2.2
Pt	-5.853 ± 0.004	3.153 ± 0.068	7.385 ± 0.016	17.3 ± 0.8	1.9

From EMT we expect that the lattice constant is $\sqrt{2}\beta s_0$, and the cohesive energy is E_0. The value for the cohesive energy, E_0, obtained from the Monte Carlo simulation, table 2, is insignificantly larger than the expected value. The heat capacity was calculated by linear regression on the cohesive energy. The calculated values for C_p are mostly larger than the harmonic value although the agreement with experimental values is not good. A preliminary analysis indicate that the system size and the small number of configurations are limiting the accuracy of the values for C_p and that the error bar deduced from the linear regression is too optimistic. The fluctuations observed in E are proportional to temperature and have the magnitude expected from the number of atoms in the system and the calculated heat capacity.

The value for the lattice constant, a, obtained by averaging over the generated configurations in the Monte Carlo simulations, table 2, is 99.4% of the experimental [33] value. The discrepancy between the lattice constant deduced from the simulations and the analytical results is due to the simplified treatment of contributions from neighbours beyond the first shell implicit in equation (3).

The fluctuations observed in a are proportional to temperature. The thermal expansion coefficient was calculated by linear regression on the lattice constant, table 2.

4. Surface energy

The surface energy is the energy of reaction per surface unit cell for the cleavage of a large crystal. The total energy after relaxation was calculated for a 512-atom supercell with 3D and 2D periodic boundary conditions. As the latter system has 2 free surfaces, the surface energy, ΔE, is

$$\Delta E = (E_{2D} - E_{3D})/2N \tag{20}$$

where N is the number of surface unit cells in each of the surfaces of the system. The calculated values are compared to the values calculated by the *linear muffin-tin orbital* (LMTO) method [34] in figure 2.

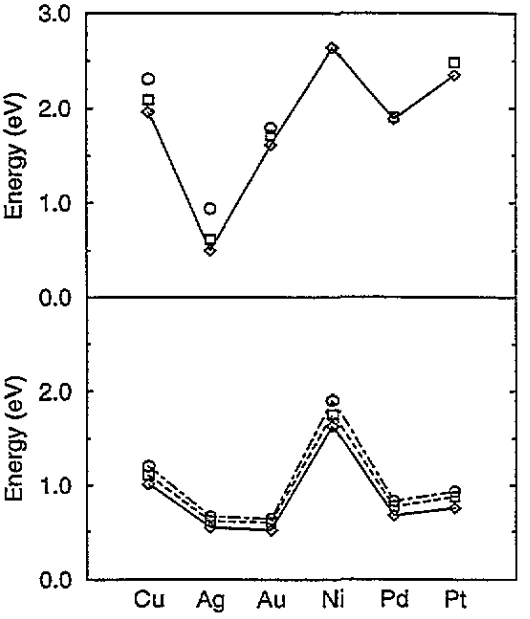

Figure 2. The surface energy in eV per surface atom calculated from LMTO [34] (upper figure) and EMT (lower figure) for the (100) (squares), (110) (circles), and (111) (diamonds) surfaces.

The comparison with the surface energies calculated from LMTO shows that EMT at the level of approximation used here gives a too low but acceptable surface energy for Cu, Ag, Ni, and Pd. However, much too low surface energies are found for Au and Pt. This could indicate that the description of Au and Pt is not adequate. However, the simulations, subsection 5.2, reproduce the experimentally observed (2×1) reconstruction of Au(110) [35, 36, 37] and Pt(110) [37, 38, 39, 40] and the preferred direction of the steps [41]. The present set of parameters for Pt also reproduces the experimentally observed patterns created by incorporation of adatoms into the surface layer of Pt(111) [17].

If the range of the EMT potential is limited to nearest-neighbour interactions, the surface energy can be calculated from the coordination number of the surface atoms, figure 1:

$$E_{100} = E_8 - E_{12} \tag{21}$$

$$E_{110} = E_{11} + E_7 - 2E_{12} \tag{22}$$

$$E_{111} = E_9 - E_{12}. \tag{23}$$

For Cu we find E_{100} = 0.439 eV, E_{110} = 0.667 eV, and E_{111}=0.332 eV. As the surface relaxation energy for Cu is small, subsection 4.1, we find agreement between the surface energies calculated from the coordination numbers and the data in figure 2.

4.1. Surface relaxation

The surface relaxation was determined by steepest-descent minimization for a system consisting of two static and 16 dynamic layers with 64 atoms in each layer.

The surface relaxation, unfortunately, depends on the number of shells included in the energy calculations. This problem is not specific for EMT, rather it will be present in any approximate total energy method, if the range of the interactions is variable.

Table 3 shows the result of optimization of the structure for Cu(100), Cu(110), and Cu(111) using different numbers of shells in the energy calculations. The oscillatory nature of the surface relaxations is only observed if the cut-off is placed between the first and the second shell.

Table 3. The surface relaxation in % and the surface relaxation energy in meV per surface atom for different choices of the cut-off in shells.

Shells	1 shell		2 shells		3 shells		5 shells	
Cu(100)	2.1%	7 meV	1.4%	10 meV	1.3%	24 meV	1.2%	21 meV
Cu(110)	5.1%	14 meV	4.2%	17 meV	3.4%	27 meV	3.4%	25 meV
Cu(111)	1.2%	4 meV	1.4%	9 meV	1.2%	17 meV	1.2%	16 meV

The results in table 4 were calculated using a cut-off after the first shell. For all the metals the relaxation is largest for the more open (110) surface and smallest for the close-packed (111) surface. Table 4 shows that large relaxations correlate with large relaxation energies.

The relaxations are largest for Au, Pt, and Pd. However, these relaxations are somewhat unrealistic as they were found for the unreconstructed surface and these surfaces are predicted to undergo a missing row reconstruction, subsection 5.2

Table 4. The surface relaxation in % and the surface relaxation energy in meV per surface atom.

	(100)		(110)		(111)	
Cu	2.1%	7 meV	5.1%	14 meV	1.2%	4 meV
Ag	2.5%	5 meV	6.7%	15 meV	1.4%	2 meV
Au	5.3%	28 meV	16.0%	79 meV	3.2%	11 meV
Ni	1.3%	9 meV	2.9%	12 meV	0.7%	6 meV
Pd	3.5%	15 meV	9.2%	40 meV	2.0%	7 meV
Pt	4.9%	36 meV	13.5%	104 meV	2.9%	14 meV

The *ab initio* values for the surface relaxations on the (100), (110), and (111) surfaces are 3.0, 9.3, and 1.3% for Cu [42, 43] and 1.3, 7, and 0.4% for Ag [42]. Except for Cu(110), where EMT gives too small a relaxation, the values calculated from EMT are in good agreement with the *ab initio* results.

4.2. Anharmonicity at the surface

The anharmonicity at the surface may be illustrated by calculation of the potential felt by an atom approaching the surface.

Figure 4 shows the potential found from a steepest-descent minimization for a system consisting of a Cu atom outside a Cu(100) surface.

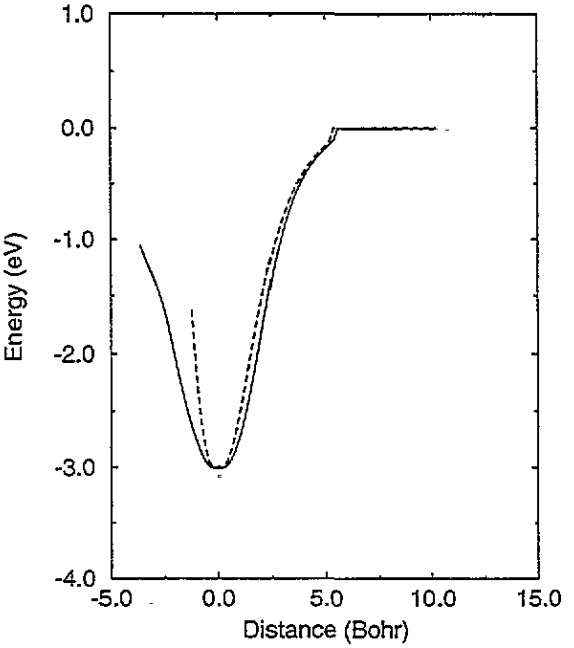

Figure 3. Potential energy of a Cu atom outside a Cu(100) surface against the distance from the equilibrium position. The dashed curve show the situation where all atoms in the substrate are static. The solid curve show the situation when the atoms in the substrate are allowed to relax.

In figures 3 and 4, the height is measured relative to the the equilibrium position of the adatom while the energy is measured relative to the situation where the atom is far from the surface.

The details of the minimization were adjusted so that the same potential energy surface was found for both adsorption and desorption of the adatom. The anomaly found near 5 Bohr above the surface is caused by the range of the potential, the determination of the potential energy surface in this region is very difficult. If the minimization is not done with sufficient care, unphysical hysteresis effects will be observed in this region.

Figure 3 shows the difference in the interaction potential found outside a static and a dynamic surface. While there is little difference in the binding energy, the potential surface outside the static surface is much stiffer than outside the dynamic surface. The softening of the potential outside the dynamic surface is due to the relaxation of the surface atoms and is important for the energy dissipation in homoepitaxy [19].

Figure 4 shows that while the stiffnesses of the potential outside the (100), (110), and (111) surfaces are very similar, the adsorption energy for the adatoms follows the expected trend, (111) < (100) < (110).

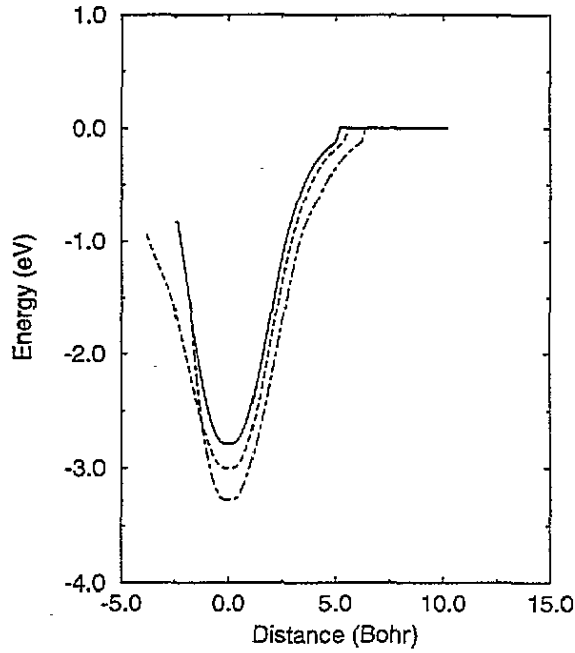

Figure 4. Potential energy of a Cu atom outside the Cu(100) (dashed curve), Cu(110) (dot–dashed curve), and Cu(111) (solid curve) surfaces against the distance from the equilibrium position.

5. Surface defects

The energy of formation for a surface defects may be calculated as a reaction energy for the reaction forming the defect in question. If the reaction is constructed so that the number of atoms is conserved and irrelevant energy terms cancel, the reaction energy is simply the difference in total energy between reactants and products.

In the following we will consider the formation of adatom–vacancy pairs, steps, and islands. For this purpose we will consider a reference system with 64 atoms per layer, six dynamic and two static layers, and 2D periodic boundary conditions. The lattice constant is fixed at the zero-temperature equilibrium value. The defects are created by addition of atoms on the free surface of this system. The formation of an additional layer is trivially calculated: we might as well add a layer of bulk atoms and the energy for adding the layer is thus NE_0, where N is the number of atoms in a layer.

5.1. Adatom–vacancy pairs

The formation energy for adatom–vacancy pairs is the reaction energy for the process

$$\text{flat surface} \rightleftharpoons \text{adatom} + \text{vacancy}. \tag{24}$$

If ϵ_n is the energy of a system with n adatoms,

$$\Delta E = \epsilon_1 + \epsilon_{-1} - 2\epsilon_0 \tag{25}$$

where $n = 0$ for the flat surface and $n = -1$ for a system with a vacancy. The results are listed in table 5. The data show that the adatom–vacancy formation energy increases

through the sequence (110) < (100) < (111). This sequence is what one would expect from a simple bond breaking argument.

Table 5. Adatom–vacancy formation energy E_{av} in eV for a relaxed surface and the difference, ΔE_{av}, in adatom–vacancy formation energy between unrelaxed and relaxed systems.

	(100)		(110)		(111)	
	E_{av}	ΔE_{av}	E_{av}	ΔE_{av}	E_{av}	ΔE_{av}
Cu	0.984	0.079	0.466	0.058	1.329	0.116
Ag	0.694	0.116	0.327	0.054	1.027	0.130
Au	0.556	0.458	0.273	0.170	1.009	0.506
Ni	1.472	0.030	0.722	0.039	1.898	0.100
Pd	0.773	0.241	0.350	0.112	1.193	0.301
Pt	0.818	0.572	0.370	0.237	1.429	0.674

The data in table 5 show that relaxations are rather important for the adatom–vacancy formation energy. The formation energy is always larger on the unrelaxed surface. On the Au, Pd, and Pt surfaces, the difference is exceptionally large, up to 670 meV, while on the other surfaces the difference is 30–130 meV. Animations show that the adatom relaxes towards the surface to compensate for the low electron density. Interestingly, while the neighbours of a surface vacancy relax away from the vacancy, the neighbours of a bulk vacancy hardly move with respect to their perfect lattice positions.

If the EMT potential is limited to nearest-neighbour interactions [16], the adatom–vacancy formation energy may be calculated from the coordination numbers of the surface atoms, e.g for a (100) surface

$$E_{av} = (E_4 - E_8) + 4(E_9 - E_8) + 4(E_7 - E_8) + 4(E_{11} - E_{12}) \tag{26}$$

where the four terms come from the adatom, the neighbours of the adatom, the neighbours of the vacancy in the first layer, and the neighbours of the vacancy in the second layer, respectively. For Cu(100) we find $E_{av} = 1.031$ eV in good agreement with the 1.063 eV found for the full calculation for the unrelaxed surface.

The p(2 × 2) and the c(2 × 2) reconstructions are closely related to the formation of adatom–vacancy pairs. Both the p(2 × 2) and the c(2 × 2) reconstructions are energetically very unfavourable for the clean metal surfaces. The lowest energy of formation is 0.14 eV for p(2 × 2) Au(110); the highest is 1.25 eV for c(2 × 2) Ni(111). The energy of formation increases through the sequence (110), (100), (111) and the energy of formation per surface unit cell is somewhat larger for c(2 × 2) than for p(2 × 2). It is worth noting that although Au(110), Pd(110), and Pt(110) are predicted to undergo a missing row reconstruction, subsection 5.2, the c(2 × 2) and p(2 × 2) reconstructions are very unfavourable for these surfaces.

5.2. Missing row reconstructions

If we take a supercell without adatoms and a supercell with an extra layer of atoms, we can redistribute the adatoms into a missing row structure. If there are N atoms in the surface layer of a supercell, the resulting system will contain N reconstructed unit cells. From the energies of the supercell without adatoms and the supercell with missing rows, we can calculate the reconstruction energy per surface unit cell:

$$\Delta E = \frac{2\epsilon_{step} - 2\epsilon_0 - NE_0}{N}. \tag{27}$$

The results are listed in table 6.

The reconstruction is most favored for the ⟨001⟩ rows on the (110) surfaces in agreement with experimental results for Au(110) [36, 37, 41] and for Pt(110) [37, 38, 39, 40] as well as calculations using EAM for Au(110) [35].

The reconstruction is least favoured for the (111) surfaces. Spontaneous formation of the ⟨001⟩ missing row reconstruction is predicted for Au(110), Pd(110) and Pt(110).

5.3. Steps

If we take a supercell without adatoms and a supercell with an extra layer of atoms, we can redistribute the adatoms into 2 strips of atoms, each strip covering 1/4 of the atoms in the original surface layer. If there are N atoms in the surface layer of a supercell, the resulting system will contain $N/2$ step atoms. From the energies of supercell without adatoms and the energy of the supercell with a strip of atoms covering half of the surface, we can calculate the reconstruction energy per step atom:

$$\Delta E = \frac{2\epsilon_{\text{step}} - 2\epsilon_0 - NE_0}{N/2} \tag{28}$$

The results are listed in table 6.

The step formation energy is smallest for steps parallel to $\langle 1\bar{1}0\rangle$ on the (110) surface and largest for steps on the (111) surface. There is a small driving force for the formation of steps on the Pt(110), Au(110), and Pd(110) surfaces. The stepped surface will be less stable than the missing row reconstruction and the steps are predicted to form kinks, subsection 5.4.

5.4. Kinks

A supercell with a strip of adatoms covering half of the surface can easily be redistributed to a system with four kinks. From the energies of the supercell with a step and the supercell with kinks, we can calculate the reconstruction energy per step atom:

$$\Delta E = \frac{\epsilon_{\text{kink}} - \epsilon_{\text{step}}}{4} \tag{29}$$

The results are listed in table 6.

For each metal the kink formation energy is about the same for steps on the (100) surface, for step edges parallel to $\langle 1\bar{1}0\rangle$ on the (110) surface, and for steps on the (111) surface, while the kink formation energy is lower for step edges parallel to ⟨001⟩ on the (110) surface.

There is a small driving force for formation of kinks on ⟨001⟩ steps on Pt(110) and Au(110).

5.5. Adatoms emitted from a step

We determine the energy increase when an atom is emitted from the step and transferred to the first reasonably stable state outside the step by a steepest-descent minimization where one of the atoms originally in the step edge is constrained to move to the terrace. The stable state is generally found in a lattice site on the terrace quite near the original position of the moving atom and in this state there is a significant interaction between the adatom and the vacancy left behind.

The results are listed in table 7. The table show that it is easier to form adatoms on stepped surfaces than to form adatoms on flat surfaces, table 5.

Table 6. Energy of formation in eV per unit cell for missing rows, steps, and kinks. For the missing row reconstructions on the (110) surfaces, MR I and MR II have rows oriented along ⟨001⟩ and ⟨1$\bar{1}$0⟩, respectively. For the steps and kinks on the (110) surfaces, Step I and Kink I refer to step edges parallel to ⟨001⟩, while Step II and Kink II refer to step edges parallel to ⟨1$\bar{1}$0⟩.

	MR I	MR II	Step I	Step II	Kink I	Kink II
Cu(100)	0.272		0.125		0.107	
Cu(110)	0.024	0.217	0.009	0.102	0.107	0.012
Cu(111)	0.441		0.208		0.107	
Ag(100)	0.187		0.085		0.082	
Ag(110)	0.001	0.162	0.000	0.076	0.079	0.003
Ag(111)	0.342		0.156		0.079	
Au(100)	0.153		0.065		0.070	
Au(110)	−0.022	0.155	−0.011	0.074	0.075	−0.008
Au(111)	0.358		0.141		0.074	
Ni(100)	0.408		0.191		0.154	
Ni(110)	0.052	0.318	0.019	0.150	0.154	0.023
Ni(111)	0.625		0.301		0.154	
Pd(100)	0.202		0.091		0.092	
Pd(110)	−0.015	0.186	−0.007	0.087	0.092	0.000
Pd(111)	0.412		0.178		0.091	
Pt(100)	0.212		0.092		0.102	
Pt(110)	−0.035	0.216	−0.018	0.103	0.107	−0.013
Pt(111)	0.500		0.198		0.104	

On the (110) surfaces the formation of adatoms from step edges parallel to ⟨1$\bar{1}$0⟩ is much harder than formation of adatoms from step edges parallel to ⟨001⟩. Except for Ni, the formation energy of adatoms from step edges parallel to ⟨1$\bar{1}$0⟩ is actually higher than the formation energy of adatoms on flat surfaces, table 5.

Table 7. Energy of formation in eV of adatoms from steps.

	(100)	⟨001⟩ step on (110)	⟨1$\bar{1}$0⟩ step on (110)	(111)
Cu	0.676	0.268	0.455	0.663
Ag	0.502	0.180	0.336	0.515
Au	0.446	0.152	0.323	0.500
Ni	0.956	0.406	0.663	0.942
Pd	0.583	0.189	0.379	0.603
Pt	0.635	0.210	0.448	0.705

5.6. Adatoms emitted from kinks

We determine the energy increase when an atom is emitted from the kink and transferred to the first reasonably stable state outside the step by the same procedure as we used to find the formation energy of adatoms emitted from steps.

For symmetry reasons the formation energy of adatoms emitted from kinks does not depend on the direction of the step on the (110) surfaces.

Comparison of tables 7 and 8 shows that the formation of adatoms is easiest from kinks on the (100) and (110) surfaces, while the adatoms are easier to form from steps on

the (111) surfaces.

Table 8. Energy of formation in eV of adatoms from kinks.

	(100)	(110)	(111)
Cu	0.507	0.239	0.714
Ag	0.364	0.163	0.555
Au	0.307	0.162	0.568
Ni	0.749	0.365	1.002
Pd	0.402	0.180	0.669
Pt	0.435	0.222	0.806

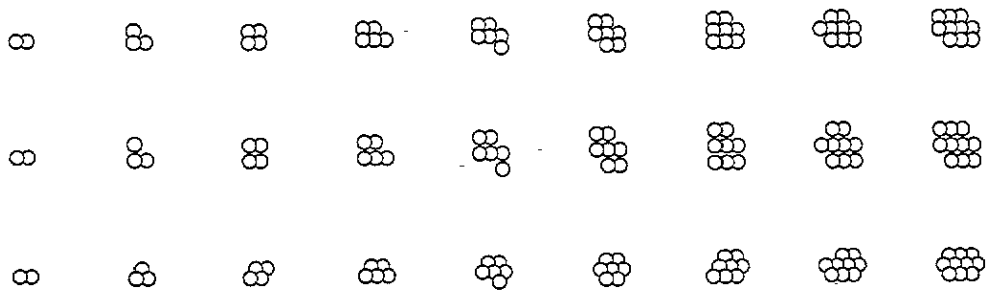

Figure 5. Islands with 2–10 atoms on (100) (upper row), (110), and (111) (lower row) surfaces.

5.7. Islands

The formation energy of islands is the reaction energy for the process

$$n \text{ adatoms} \rightleftharpoons n\text{-atom island.} \tag{30}$$

If ϵ_n is the energy of a system with n adatoms,

$$\Delta\epsilon_n = \epsilon_n + (n-1)\epsilon_0 - n\epsilon_1. \tag{31}$$

It is an almost trivial result that the simulations show that islands are more stable than isolated adatoms for all the metals and all surfaces.

The dissociation energy of islands is the reaction energy for the process

$$n\text{-atom island} \rightleftharpoons (n-1)\text{-atom island} + \text{adatom} \tag{32}$$

If E_n is the energy of a system with n adatoms,

$$\Delta E_n = E_{n-1} + E_1 - E_n - E_0. \tag{33}$$

The dissociation energy depends on the actual configuration chosen for the island. For some of the islands shown in figure 5 there is a huge number of isomers.

The results are listed in table 9. The table shows that while most islands are stable with respect to emission of adatoms, the trimer and the hexamer are not stable on the Au(110), Pd(110), and Pt(110) surfaces. This does not necessarily mean that there are no stable islands with three or six atoms on these surfaces; some other isomers might be more stable than the isomer shown in figure 5.

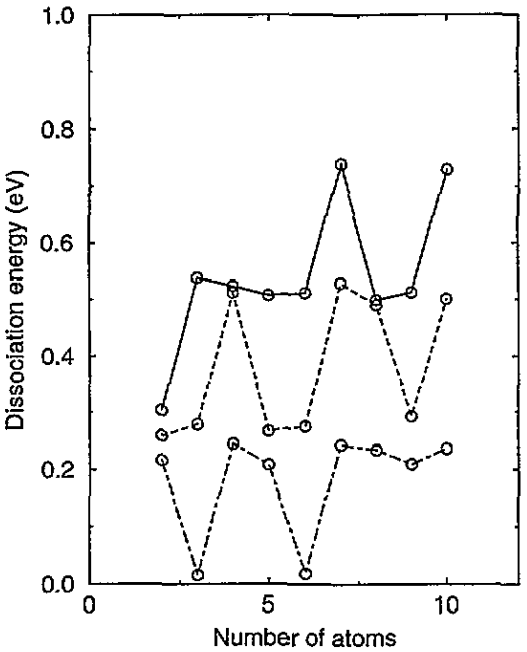

Figure 6. Dissociation energy (eV) for islands with 2–10 atoms on Cu(100) (dashed), Cu(110) (dot–dashed), and Cu(111) (solid).

Table 9. Dissociation energy (eV) for islands.

	Dimer	Trimer	Tetramer	Pentamer	Hexamer	Heptamer
Cu(100)	0.259	0.279	0.511	0.267	0.275	0.528
Cu(110)	0.216	0.016	0.245	0.208	0.018	0.243
Cu(111)	0.303	0.538	0.523	0.507	0.511	0.739
Ag(100)	0.191	0.195	0.382	0.182	0.194	0.375
Ag(110)	0.174	0.001	0.177	0.164	0.001	0.175
Ag(111)	0.256	0.441	0.420	0.408	0.408	0.584
Au(100)	0.160	0.134	0.319	0.129	0.148	0.290
Au(110)	0.185	−0.020	0.160	0.166	−0.017	0.154
Au(111)	0.284	0.481	0.440	0.428	0.414	0.594
Ni(100)	0.370	0.418	0.739	0.401	0.413	0.779
Ni(110)	0.316	0.046	0.372	0.310	0.046	0.373
Ni(111)	0.404	0.733	0.716	0.705	0.706	1.032
Pd(100)	0.228	0.217	0.442	0.200	0.221	0.419
Pd(110)	0.210	−0.013	0.200	0.190	−0.012	0.192
Pd(111)	0.311	0.536	0.505	0.483	0.481	0.692
Pt(100)	0.251	0.213	0.475	0.202	0.233	0.431
Pt(110)	0.249	−0.029	0.223	0.223	−0.030	0.211
Pt(111)	0.412	0.688	0.631	0.609	0.589	0.847

6. Diffusion

The activation energy for diffusion is determined by steepest-descent minimization where the diffusing atom is constrained to move from one relaxed lattice site to another.

In the present manuscript we are using EMT at its lowest level of approximation and we

will limit the discussion to phenomena that can be treated using this level of approximation. Among the phenomena that we cannot treat are the covalent effects important for the exchange mechanism of diffusion for adatoms on flat surfaces [10, 44, 45].

6.1. Diffusion of vacancies

Before we consider the diffusion of adatoms, we will briefly consider the diffusion of vacancies on flat surfaces, table 10.

Table 10. Activation energy (eV) for vacancy diffusion.

	(100)	(110) $(1\bar{1}0)$	(110) ⟨001⟩	(111)
Cu	0.437	0.506	0.921	0.618
Ag	0.417	0.460	0.781	0.536
Au	0.520	0.470	0.890	0.455
Ni	0.562	0.705	1.240	0.910
Pd	0.572	0.584	0.991	0.632
Pt	0.773	0.704	1.250	0.688

While the activation energies for diffusion of adatoms, table 11, and of vacancies, table 10, are close on the (100) surfaces, the activation energy for vacancy diffusion is higher than the activation energy for adatom diffusion on the (110) and in particular on the (111) surfaces.

6.2. Adatom diffusion on flat surfaces

Table 11. Activation energy (in eV) for diffusion on an adatom on a flat surface. The numbers in parenthesis are the activation energies found on a static substrate.

	(100) jump	(110) $(1\bar{1}0)$ jump	(110) ⟨001⟩ jump	(110) ⟨001⟩ exchange	(111) jump
Cu	0.425 (0.436)	0.292 (0.471)	0.826 (0.842)	0.419	0.053 (0.094)
Ag	0.365 (0.380)	0.291 (0.420)	0.639 (0.661)	0.561	0.064 (0.091)
Au	0.490 (0.499)	0.268 (0.473)	0.670 (0.768)	0.554	0.102 (0.126)
Ni	0.558 (0.581)	0.407 (0.649)	1.157 (1.164)	0.564	0.068 (0.121)
Pd	0.503 (0.505)	0.366 (0.544)	0.776 (0.824)	0.599	0.104 (0.129)
Pt	0.689 (0.704)	0.420 (0.695)	0.945 (1.065)	0.809	0.159 (0.187)

The activation energy for adatom diffusion on Cu(100) is 0.425 eV which is marginally larger than the the experimental value, 0.39 eV [46, 47]; also on Ni(110) the calculated value, 0.407 eV is larger than the experimental value, 0.32 eV, [48].

For diffusion on static surfaces the activation energy is always higher, by up to 275 meV for Pt(110), than if all atoms in the substrate are dynamic. For all metals we find that the activation energy for the jump mechanism increases through the sequence (111), (110) long bridge, (100), and (110) short bridge. For diffusion across the close-packed rows on the (110) surface, the exchange mechanism has a lower activation energy than the jump mechanism [44], although the activation energy for the exchange mechanism across the close-packed rows is much higher than the activation energy for diffusion by the jump mechanism along the close-packed rows.

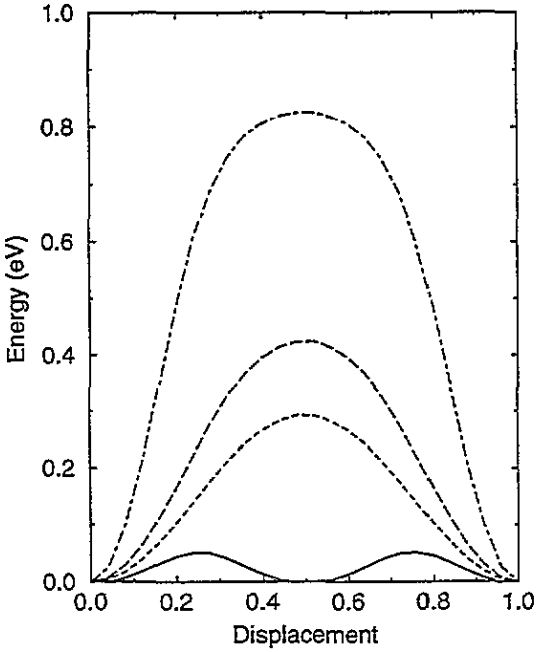

Figure 7. Potential energy of an adatom diffusing on Cu(100) (long-dashed curve), Cu(110) $\langle 1\bar{1}0\rangle$ (dashed-curve), Cu(110) $\langle 001\rangle$ (dot–dashed curve), Cu(111) (solid curve). For each of the graphs, the displacement has been normalized by the distance between equilibrium positions. The minimum in the middle of the Cu(111) curve is due to the HCP site.

Liu *et al* [49] have examined the activation energies for adatom diffusion using the *embedded atom method* (EAM). Except for Pt, where the EAM gives significantly lower activation barriers for diffusion, the values in table 11 are in good agreement with the data of Liu *et al*. A recent Car–Parinello simulation [50] gives much higher activation energies for adatom diffusion on Cu(100) than found by EMT or EAM.

When the metals are ordered according to their activation energy, somewhat different sequences are found for the different surfaces. However, Ag shows the lowest activation energy among the metals for all surfaces and Pt, Pd, and Ni have the highest activation energies.

In the jump mechanism for adatoms on flat surfaces relaxations are important and the activation energy has roughly equal contributions from the relaxations, from the energy changes in the adatom, and from energy changes in the substrate atoms. Figure 8 show the activation energy for adatom diffusion on Ag(100) and a breakdown of this activation energy into some of its components. The largest single component is due to the energy change for the diffusing atom as one would intuitively expect. The contribution from bond breaking in the first layer is built up from two contributions. The bond breaking gives a positive contribution which sets in earlier than the negative contribution from the bond formation. The sum of these contributions gives the bell shaped contribution, C, in figure 8. Interestingly, there is a large and negative contribution from the relaxations in the substrate. The contribution from the relaxations is broader than the contribution from the energy changes in the diffusing atom. On a static substrate the barrier is thus not only higher, it also has a different, wider shape. At the peak maximum the contribution from the relaxations and the contribution from from bond breaking in the first layer are approximately

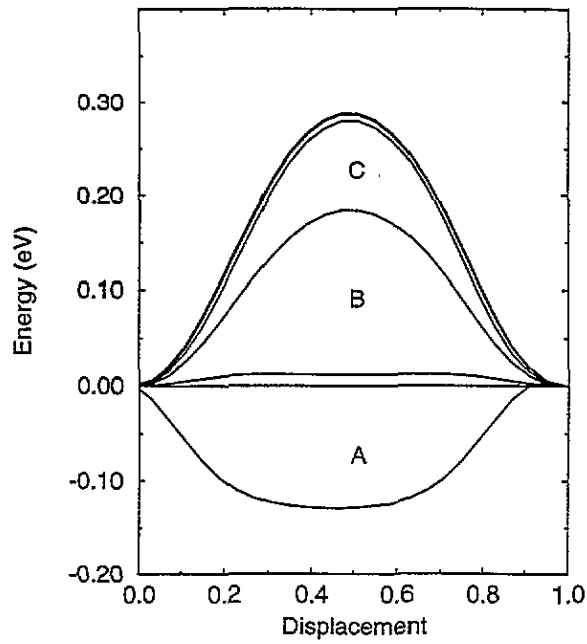

Figure 8. The activation energy for diffusion on Ag(100) is shown as the bold curve. The contribution A is due to relaxations in the substrate, B is due to the diffusing atom, and C is due to bond breaking and bond formation in the first layer. The contribution between A and B is due to bond breaking and bond formation in the second layer. The contribution between C and the bold curve is the contribution which cannot be accounted for in this description.

$\frac{2}{3}$ and $\frac{1}{2}$, respectively, of the contribution from the energy change of the adatom.

6.3. Adatoms emitted from a step

The activation energy for emission of an atom from a step is determined from steepest-descent minimization, subsection 5.5. The emission of an adatom from a step leaves behind a vacancy in the step edge and is thus expected to have a rather high activation energy.

The activation barriers for Cu are shown in figure 9. Detailed examination of the data from the simulations shows that for all metals and all surfaces the activation barriers have a simple bell shape. The activation barriers for all the metals are summarized in table 12.

Table 12. Activation energy (in eV) for diffusion of an atom out of a step.

	(100)	(110) $\langle 1\bar{1}0\rangle$	(110) $\langle 001\rangle$	(111)
Cu	0.848	0.534	1.169	0.770
Ag	0.722	0.455	0.919	0.629
Au	0.811	0.407	0.958	0.559
Ni	1.125	0.773	1.638	1.105
Pd	0.922	0.541	1.100	0.736
Pt	1.152	0.608	1.349	0.820

The activation energy increases through the sequence Ag, Au, Pd, Cu, Pt, Ni and through the sequence $\langle 1\bar{1}0\rangle$ (110), (111), (100), and $\langle 001\rangle$ (110).

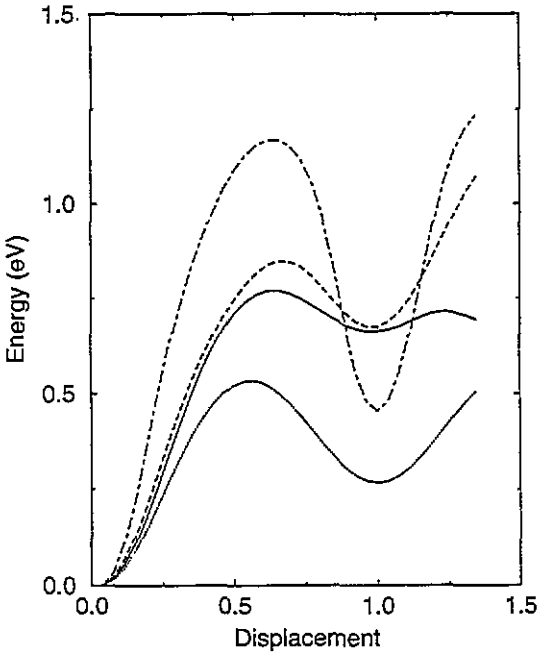

Figure 9. Potential energy of an adatom diffusing out of a step on Cu(100) (dashed curve), a $\langle 1\bar{1}0\rangle$ step on Cu(110) (dotted), a $\langle 001\rangle$ step on Cu(110) (dot–dashed curve), and a step on Cu(111) (solid curve). For each of the graphs, the displacement has been normalized by the distance between equilibrium positions.

6.4. Diffusion over a step

The activation barriers for diffusion over a step edge for Cu are shown in figure 10. The activation energies calculated for the over edge and for the exchange mechanisms are listed in tables 13 and 14 respectively. For the (100) surfaces the activation barrier has no features. For the *over edge* mechanism on the $\langle 001\rangle$ step on the (110) surface, the adatom moves over the edge in a *long-bridge* geometry into an *on top* geometry on the terrace. The stabilities of the two geometries are comparable and for some of the metals a poorly defined energy minimum is found near the *on top* geometry.

The barrier for the *over edge* mechanism on the $\langle 1\bar{1}0\rangle$ step on a (110) surface is not clearly resolved as the diffusing atom drops down in an unstable *on top* geometry on the terrace.

For the *over edge* mechanism on the (111) surface, there is first a little minimum corresponding to the HCP site. The transition state occurs after the diffusing atom has moved into the HCP site on the terrace but before it reaches the FCC site. The resulting activation barrier is unusually asymmetric.

For the *exchange* mechanism on the (111) surface the activation barrier is symmetric, both moving atoms move between FCC sites. However, the transition state has a low symmetry and a complicated geometry. A local minimum is seen when the diffusing atom continues through the HCP site.

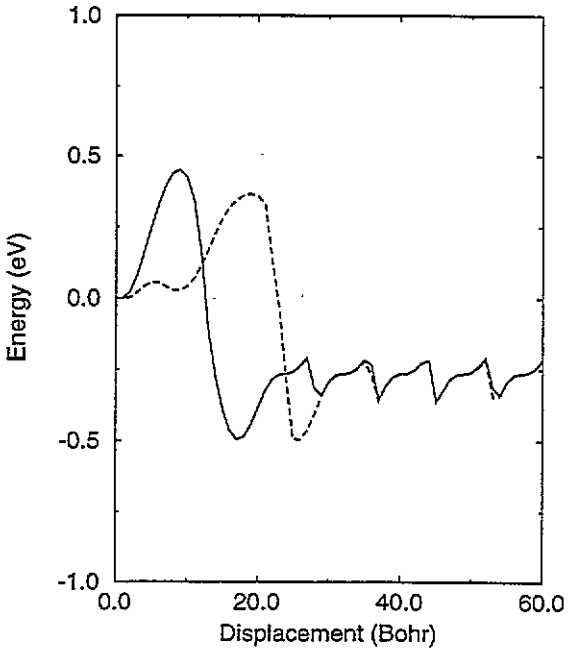

Figure 10. Potential energy surface for the exchange mechanism (solid) and over edge mechanism (dashed) on Cu(111). The local minimum on the barrier for the over edge mechanism is due to the atom moving into an HCP site.

Table 13. Activation energy (in eV) for diffusion of an atom over a step. Over edge mechanism. The barrier for diffusion over a $\langle 1\bar{1}0\rangle$ step on the (110) surfaces cannot be resolved on Au(110) and Pt(110).

	⟨100⟩	(110) $\langle 1\bar{1}0\rangle$ step	(110) ⟨001⟩ step	111
Cu	0.572	0.48	0.840	0.365
Ag	0.450	0.36	0.646	0.359
Au	0.546		0.675	0.260
Ni	0.787	0.68	1.178	0.529
Pd	0.573	0.42	0.779	0.306
Pt	0.755		0.944	0.363

Table 14. Activation energy (in eV) for diffusion of an atom over a step by the exchange mechanism.

	⟨100⟩	(110) ⟨001⟩	(110) ⟨001⟩	⟨111⟩
Cu	0.626	0.574	0.690	0.450
Ag	0.559	0.537	0.605	0.455
Au	0.528	0.582	0.691	0.326
Ni	0.890	0.810	0.917	0.669
Pd	0.698	0.658	0.777	0.478
Pt	0.797	0.782	1.294	0.470

6.5. Diffusion along a step

The activation barrier for diffusion parallel to a step is exemplified for Cu in figure 11 and summarized for all the metals in table 15.

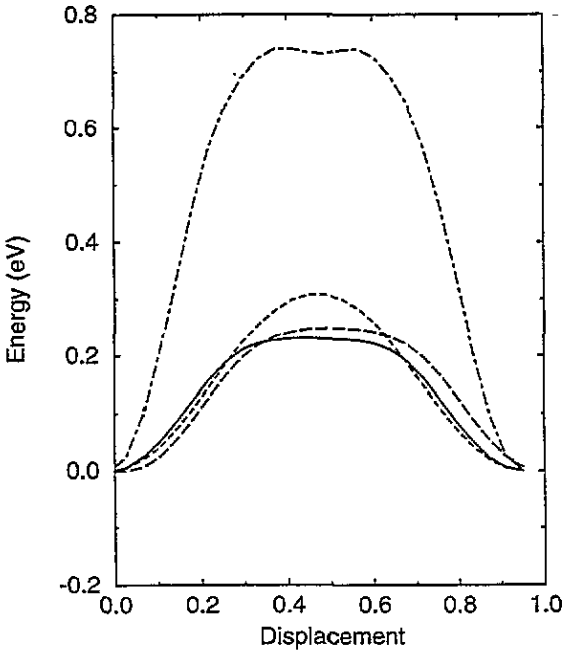

Figure 11. Potential energy of an adatom diffusing along a step on Cu(100) (long-dashed curve), along the $\langle 1\bar{1}0\rangle$ direction on Cu(110) (dashed curve), along the $\langle 001\rangle$ direction on Cu(110) (dot–dashed curve), and on Cu(111) (solid curve). For each of the graphs, the displacement has been normalized by the distance between equilibrium positions.

There is a double-peak structure in the activation barrier for diffusion along $\langle 001\rangle$ on the (110) surface, figure 11. The diffusing atom moves so much vertically that it interacts significantly with two close-packed rows midway in the diffusion event.

The double-peak structure for diffusion on the (111) surface is due to the existence of both FCC and HCP sites on this surface.

Table 15. Activation energy (in eV) for diffusion of an atom along a step.

	$\langle 100\rangle$	$\langle 110\rangle$ $\langle 001\rangle$ step	$\langle 110\rangle$ $\langle 1\bar{1}0\rangle$ step	111
Cu	0.247	0.307	0.740	0.228
Ag	0.224	0.299	0.652	0.220
Au	0.302	0.291	0.797	0.311
Ni	0.330	0.431	1.000	0.296
Pd	0.308	0.380	0.869	0.310
Pt	0.438	0.448	1.110	0.456

For Cu(100) experiments [46, 47] show that an adatom diffuses faster along steps than on the terrace in agreement with the lower activation barrier for diffusion along steps, tables 11 and 15.

6.6. Emission of adatoms from a kink

The activation barriers for emission of an adatom from a kink on the Cu surfaces are shown in figure 12. The activation energies for diffusion of the kink atom to the terrace and along

the step are listed in tables 16 and 17, respectively. For the (100) and (110) surfaces, detailed examination of the data from the simulations shows that the diffusion process is uncomplicated. However, for the (111) surface, the diffusing atom moves through an HCP geometry before reaching the transition state. The HCP site is not detectable in the energy profile and the minimum is found at the FCC site.

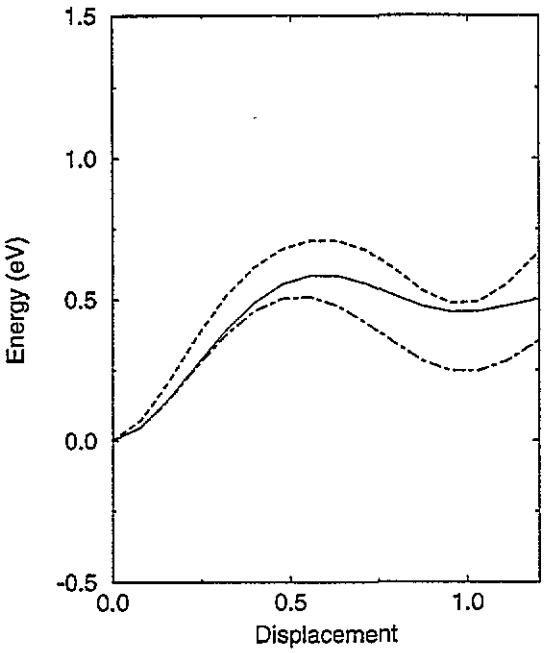

Figure 12. Potential energy of an adatom diffusing out of a kink on Cu(100) (dashed curve), Cu(110) (dot–dashed curve), Cu(111) (solid curve). For each of the graphs, the displacement has been normalized by the distance between equilibrium positions.

Table 16. Activation energy (in eV) for diffusion of an atom out of a kink.

	(100)	(110) ⟨001⟩ step	(110) ⟨1$\bar{1}$0⟩ step	(111)
Cu	0.706	0.985	0.508	0.583
Ag	0.605	0.770	0.441	0.482
Au	0.698	0.782	0.409	0.420
Ni	0.967	1.393	0.732	0.851
Pd	0.781	0.929	0.540	0.570
Pt	1.009	1.150	0.612	0.631

7. Conclusions

In the present manuscript we have demonstrated that approximate total energy methods may be used in extensive calculations of the stability and dynamics of surface defects.

While EMT by construction reproduces the cohesive energy and the present set of parameters gives good agreement with the experimental results for the bulk thermal expansion, with *ab initio* calculations of the surface relaxation, and, for some of the metals,

Table 17. Activation energy (in eV) for diffusion of an atom along a kink.

	(100)	(110) $(1\bar{1}0)$ step	(110) (001)	(111)
Cu	0.455	0.505	0.763	0.438
Ag	0.390	0.455	0.646	0.386
Au	0.455	0.430	0.786	0.456
Ni	0.620	0.713	1.045	0.590
Pd	0.504	0.563	0.866	0.504
Pt	0.654	0.676	1.105	0.667

with *ab initio* values for the surface energy, the calculated values for the surface energy of Au and Pt are clearly too low. While this is not necessarily too serious for the calculated stability of surface defects, some caution is required and we will limit the conclusions to results that do not depend on the details of the potential or on the exact values of the parameters.

For a static substrate the adsorption potential is much too steep, the formation energy for adatom–vacancy pairs is too high, and the activation energy for diffusion of adatoms is too high, in particular along the $\langle 1\bar{1}0 \rangle$ direction on the (110) surfaces.

The surface energies, the surface relaxation, and the surface relaxation energy increase through the sequence (111), (100), (110). The formation energy of defects increases through the sequence *steps*, *kinks* and *missing row* reconstructions, *adatom–vacancy pairs*.

For adatom diffusion on terraces the change in energy for the diffusing atom, the change in energy in the surrounding atoms, and the change in energy due to relaxations give approximately equal contributions to the activation energy. The contribution from the relaxations both decreases the maximum and changes the shape of the barrier.

Acknowledgments

Many discussions with Jens K Nørskov, Karsten W Jacobsen and Ivan Stensgaard are gratefully acknowledged.

References

[1] Jacobsen K W, Nørskov J K and Puska M J 1987 *Phys. Rev.* B **35** 7423
[2] Jacobsen K W 1988 *Comment. Condens. Matter Phys.* **14** 129
[3] Chetty N, Jacobsen K W, and Nørskov J K 1991 *J. Phys. C: Solid State Phys.* **3** 5437
[4] Chetty N, Stokbro K, Jacobsen K W, and Nørskov J K 1992 *Phys. Rev.* B **46** 3798
[5] Stave M S, Sanders D E, Raeker T J and DePristo A E 1993 *J. Chem. Phys.* **93** 4413
[6] Daw M S and Baskes M I 1983 *Phys. Rev. Lett.* **50** 1285
[7] Ercolessi F, Tosatti E and Parinello M 1986 *Phys. Rev. Lett.* **57** 719
[8] Rose J H, Ferrante J and Smith J R 1981 *Phys. Rev. Lett.* **47** 675
[9] Finnis M W and Sinclair J E 1984 *Phil. Mag. A* **50** 45
[10] Hansen L, Stoltze P, Jacobsen K W and Nørskov J K 1991 *Phys. Rev.* B **44** 6523
[11] Nørskov J K and Jacobsen K W 1987 *The Structure of Surfaces II (Springer Series in Surface Science II)* ed J F van der Veen and M A van Hove (New York: Springer) p 118
[12] Jacobsen K W and Nørskov J K *Phys. Rev. Lett.* **59** 2764
[13] Jacobsen K W and Nørskov J K 1988 *Phys. Rev. Lett.* **60** 2496
[14] Ditlevsen P D, Stoltze P and Nørskov J K 1991 *Phys. Rev.* B **44** 13 002
[15] Jacobsen K W and Nørskov J K 1990 *Phys. Rev.* B **65** 1788
[16] Jacobsen K W and Stoltze P 1991 *Ordering at Surfaces and Interfaces (Springer Series in Materials Science 17)* ed A Yoshimori, T Shinjo and H Watanabe (Berlin: Springer) p 187

[17] Jacobsen J, Jacobsen K W and Stoltze P 1994 *Preprint*
[18] Nørskov J K, Jacobsen K W, Stoltze P and Hansen L 1993 *Surf. Sci.* **283** 277
[19] Stoltze P and Nørskov J K 1993 *Phys. Rev.* B **48** 5607
[20] Stoltze P, Jacobsen K W and Nørskov J K 1987 *Phys. Rev.* B **36** 5035
[21] Hansen L B, Stoltze P, Nørskov J K, Clausen B S and Niemann W 1990 *Phys. Rev. Lett.* **64** 3155
[22] Hansen L B, Stoltze P, Jacobsen K W and Nørskov J K 1993 *Surf. Sci.* **289** 68
[23] Clausen B S, Gråbæk L, Topsöe H, Hansen L B, Stoltze P, Nørskov J K and Nielsen O H 1993 *J. Catal.* **141** 368
[24] Christensen O B, Ditlevsen P, Jacobsen K W, Stoltze P, Nielsen O H and Nørskov J K 1989 *Phys. Rev.* B **40** 1993
[25] Christensen O B, Stoltze P, Jacobsen K W and Nørskov J K 1990 *Phys. Rev.* B **41** 12413
[26] Chakraborty B, Xi Z G, Jacobsen K W, and Nørskov J K 1992 *J. Phys.: Condens. Matter* **4** 7191
[27] Stoltze P, Nørskov J K and Landman U 1988 *Phys. Rev. Lett.* **61** 440
[28] Stoltze P, Nørskov J K and Landman U 1989 *Surf. Sci.* **220** L693
[29] Stoltze P 1990 *J. Chem. Phys.* **92** 6306
[30] Denier van der Gon A W, Frenkel D, Frenken J W M, Smith R J and Stoltze P 1991 *Surf. Sci.* **256** 385
[31] Nielsen O H, Sethna J P, Stoltze P, Jacobsen K W and Nørskov J K 1994 *Europhys. Lett.* **26** 51
[32] Stoltze P and Nørskov J K 1991 *The Structure of Surfaces III (Springer Series in Surface Science 24)* ed S Y Tong, M A van Hove, K Takayanagi and X D Xie (Berlin: Springer) p 19
[33] Emsley J 1991 *The Elements* 2nd edn (Oxford: Oxford University Press)
[34] Skriver H and Rosengaard N 1992 *Phys. Rev.* B **46** 7157
[35] Roelofs L D, Foiles S M, Daw M S and Baskes M I 1990 *Surf. Sci.* **234** 63
[36] Moritz W, Wold D 1985 *Surf. Sci.* **103** L655
[37] Vlieg E, Robinson I K and Kern K 1990 *Surf. Sci.* **233** 248
[38] Kellogg G L 1985 *Phys. Rev. Lett.* **55** 2168
[39] Niehus H 1984 *Surf. Sci.* **145** 407
[40] Korte U and Meyer-Ehmsen G 1992 *Surf. Sci.* **271** 616
[41] Zimmermann H, Nold M, Rumahn U, Göbel H von Blanchenhagen P and Schommers W 1993 *Surf. Sci.* **297/288** 876
[42] Bohnen K P, Th. Rodach and Ho K M 1991 *The Structure of Surfaces (Springer Series in Surface Science 24)* ed S Y TongY, M A van Hove, K Takayanagi and X D Xie (Berlin: Springer) p 16
[43] Ho K M, Bohnen K P 1985 *Phys. Rev. Lett.* **32** 3446
[44] Feibelman P 1990 *Phys. Rev. Lett.* **65** 729
[45] Gravil P A and Holloway S 1994 *Surf. Sci.* **310** 267
[46] Breeman M and Boerma D O 1992 *Surf. Sci.* **269/270** 224
[47] Breeman M and Boerma D O 1980 *Surf. Sci.* **287/288** 881 (1003)
[48] Tung R T and Graham W R *Surf. Sci.* **97** 73
[49] Liu C L, Cohen J M, Adams J B and Voter A F 1991 *Surf. Sci.* **253** 334
[50] Lee C, Barkema G T, Breeman M, Pasquarello A and Car R 1994 *Surf. Sci.* **306** L575